

INVESTIGATION OF INFLUENCE OF ATOMIC VACANCY DEFECTS ON VIBRATIONAL CHARACTERISTICS OF CARBON NANOTUBES

Surinder Kumar

Department of Mechanical Engineering, Sant Longowal Institute of Engineering and Technology Longowal

Abstract

Due to high strength, stiffness and light weight, carbon nanotubes have wider scope as promising candidate for nanomechanical resonators. Any atomic vacancy defect means the absence of the atoms at particular location, which affect the sensing performance and dynamic behavior. In this paper a molecular structural mechanics investigation has been carried out to explore the influence of the defects on vibrational characteristics of single walled carbon nanotubes. These defects are simulated by removing atoms from single walled carbon nanotubes to bring the artificial situation closer to reality. Cantilevered armchair and zigzag nanotubes with various aspect ratios are considered for dynamic analysis. The effect of different vacancy defects and their position over the tube length on the natural frequency of armchair and zigzag nanotubes is investigated. Finally the present results are compared with continuum structure mechanics and molecular structural mechanics approach of previously published research papers and found present work is in good agreement with previously carried out works.

Key Words: Vacancy defects, carbon nano-tubes, vibration characteristics, zigzag, armchair

1. INTRODUCTION

Carbon nanotubes are the excellent material for advance Nanoelectromechanical sensors (NEMS) and actuators due to their high stiffness and light weight. These features of CNTs result high vibrational frequencies. Vibrational behavior of CNTs is the fundamental characteristic that should be studied, because it is essential for the applications such as NEMS devices. Gibson et. al. studied vibrational behavior of CNTs and their composites theoretically and experimentally [1]. Using continuum structural mechanics approach Joshi et. al. [2] investigated the effect of artificial defects on vibrational characteristics of the single walled carbon nanotubes (SWCNTs) of various lengths and diameters. Li and Chou [3] studied the fundamental frequencies of SWCNTs using atomistic modeling based on molecular structural mechanics. Gao et.al. [4] investigated the fundamental resonance frequency of SWCNTs with large aspect ratio lies in MHz range. Joshi et. al. [5] has investigated the effect of position of nanoparticle along the length of the nanotube and results are compared with numerical data obtained by Rayleigh Ritz method. The use of SWCNT as bio sensors has been recently instigated using FEM simulation by Gupta et al. [6]. Chowdhury et. al. [7] also examined CNTs as bio sensors using numerical method based on continuum structural mechanics. Mielke et.

al. [8] utilized density function theory and semi empirical methods, and molecular structural mechanics calculations with Tersoff Brenner potential to explore the roll of the atomic vacancy defects in the fracture of carbon nanotube under axial tension. Georgantzinos and Anifanties [9] reported vibrational characteristics of multiwalled carbon nanotubes (MWCNTs) using spring and lumped masses for various boundary constraints. In another work [10] they investigated vibrational behavior of CNTs and mass sensitivity of MWCNTs when a nanoparticle attached with them utilizing spring mass based finite element formulations. They found that, due to frequency shift of the basic modes MWCNTs have ability not only to sense the added mass, but also detect its weight and position over the length of nanotube. Mir et. al. [11] and Sakhaee-Pour et.al [12] examined the vibrational behavior of bridged and cantilever single walled carbon nanotubes with different length and diameters using finite element methods with beam elements in their simulations.

In recent years, large number of research activities has been done to study the nanostructures. Various observation based on experimental study have been reported the existence of geometric defects, such as Stone-Wales (SW) defect and atomic vacancy defects in CNTs [13]. Considerable theoretical studies have been carried out the defect-induced degradation in the mechanical properties of CNTs. Based on literature search, most paper focused on the effect of defects on fracture mechanism of CNTs under axial loadings [14-18]. Parvanesh et al. [19] developed a structural model to analyze natural frequency of single-walled carbon nanotubes under fixed-fixed and fixed-free boundary configuration. They examined influence of mono and diatomic vacancy and Stone-Wales defects on the natural frequency of zigzag and armchair CNTs of various aspect ratios. The effect of Stone-Wales defects on behavior and fracture mechanism of armchair, zigzag and chiral SWCNTs subjected to axial tension has also examined [20]. Number of different defects has been investigated on the surface of carbon nanotubes, which were the result of synthesis process. A few defects are large enough, through which even C60 molecules or metal molecules can pass. Molecular structural mechanics investigation has been done to examine the influence of number of different vacancy defects on buckling and tensile strength of the SWCNTs of different chirality [21]. The bending rigidity of CNTs has been affected by number and type of defects. A theoretical study with empirical potential function has been done on defective and perfect CNTs based on molecular structural mechanics approach [22]. However, a single defect has been considered in this study. Fig.1 shows the image of single-walled carbon nanotube under transmission electron microscopes (TEM)

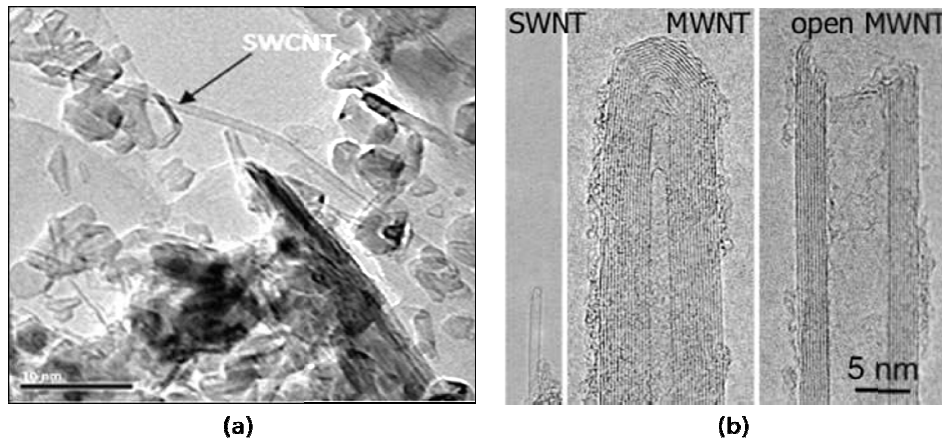
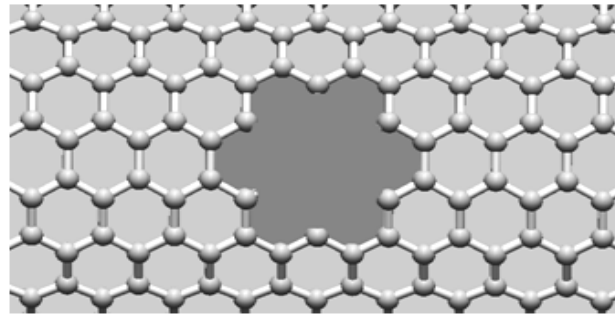


Fig. 1 Transmission electron microscopic image of carbon nanotubes [2]

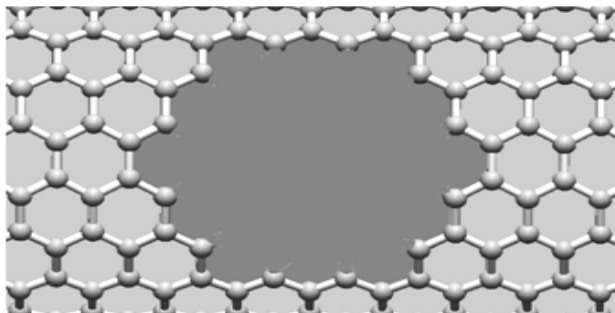
Effect of single atom vacancy defects or under defective support constraint on the vibrational frequency of basic mode shapes has been reported [23]. A comparison of frequency shift of defective and perfect, zigzag and armchair CNTs of same length has also been reported. Kumar and Harsha [24] examined the utility of multiwalled carbon nanotubes as bio sensors using continuum structural mechanics approach. It is observed [25-27] that the atomistic molecular structural mechanics approach reliable as compared to continuum structural mechanics based methods as consequences of implementing interactions at the atomic scale.

Anifantis et.al. investigated mass sensing potential of multi-walled carbon nanotubes. A comparison has been carried out to observe whether multiwalled carbon nanotubes are more or less sensitive to added mass as compared to single-walled carbon nanotubes having the same aspect ratios (length/diameter). A significant variation in frequency shift for various attached masses onto CNTs has been observed from the analysis and data available [10]. A higher frequency shift has been observed in single-walled carbon nanotubes than multi-walled carbon nanotubes.

In the present paper, 3-dimensional atomistic finite element model is used to simulate the atomic structure of the defective SWCNT considering atomic vacancy defects (type A and type B). The vibrational behavior of armchair (11,11) and zigzag(19,0) single walled carbon nanotubes of various aspect ratios ($L/d=10, 15$ and 20) with various types of atomic vacancy defects is investigated based on molecular structural mechanics approach. The influence of the numbers of defects and their position along the length of the SWCNT of various aspect ratios are also examined. In present work number of defect considered are 1, 3, 5 and 7, and the dimensionless positions (x/L) of defect along the length of SWCNTs are considered as 0.1, 0.3, 0.5, 0.7 and 0.9. Types of vacancy defects consider in the present paper are shown in Fig.2.



(a)



(b)

Fig. 2. Schematic diagram of atomic vacancy defect model (a) Type A defect: lack of six atoms. (b) Type B defect: lack of twenty four atoms.

There are two types of defects are considered in present paper

- Defect type A
- Defect type B

Type A defects are having 6 carbon atoms missing and defect B 24 carbon atoms are missing from a particular location on CNTs as shown in Fig. 2(a) and (b). These defects are uniformly distributed along the length of armchair CNTs as shown in Fig. 3 and zigzag CNT in Fig. 4.

Influence of position of the defect along the length of the both armchair and zigzag CNTs is also investigated.

Defective CNT models used by Joshi et. al. [2] is shown in Fig. 5.

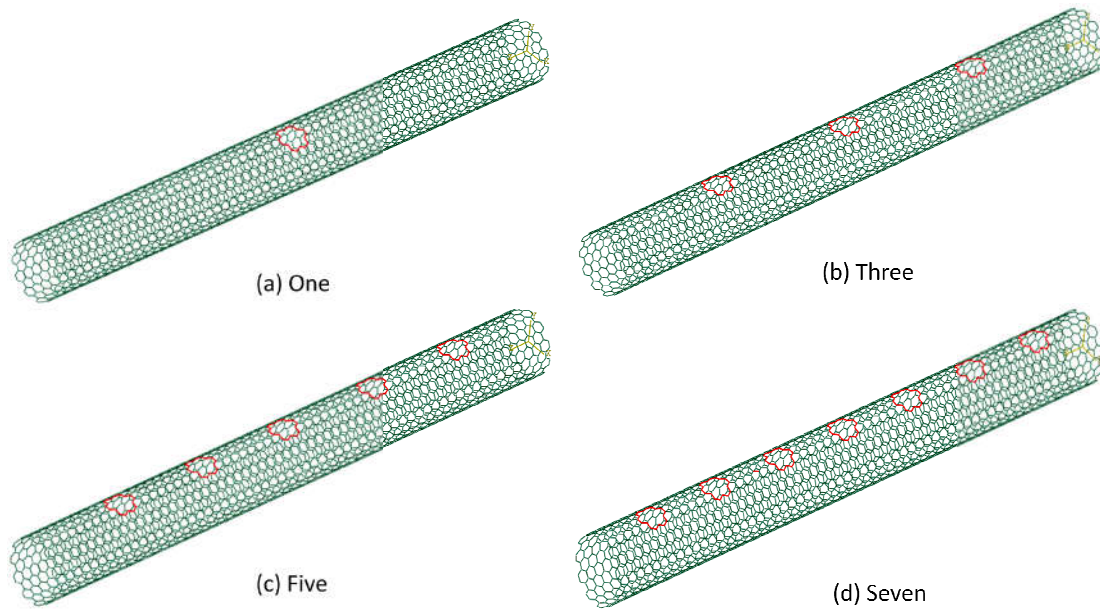


Fig.3. Defects on armchair (11,11) CNTs: (a) Single defect, (b) Three defects, (c) Five defects (d) Seven defects

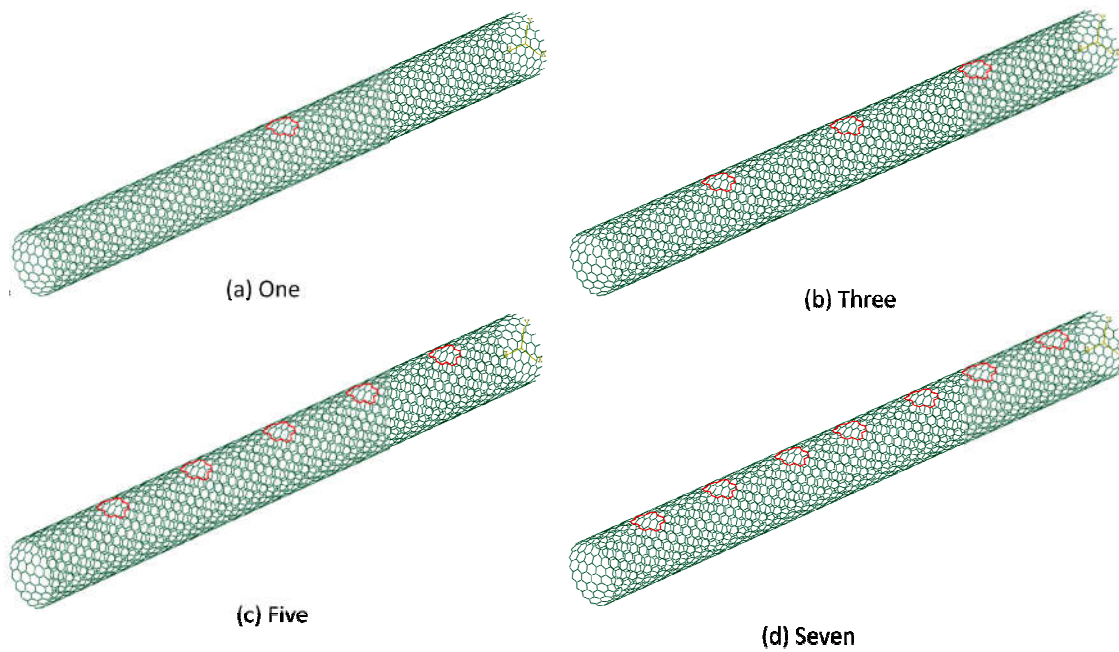


Fig.4. Defects on zigzag (19,0) CNTs: (a) Single defect, (b) Three defects, (c) Five defects (d) Seven defects

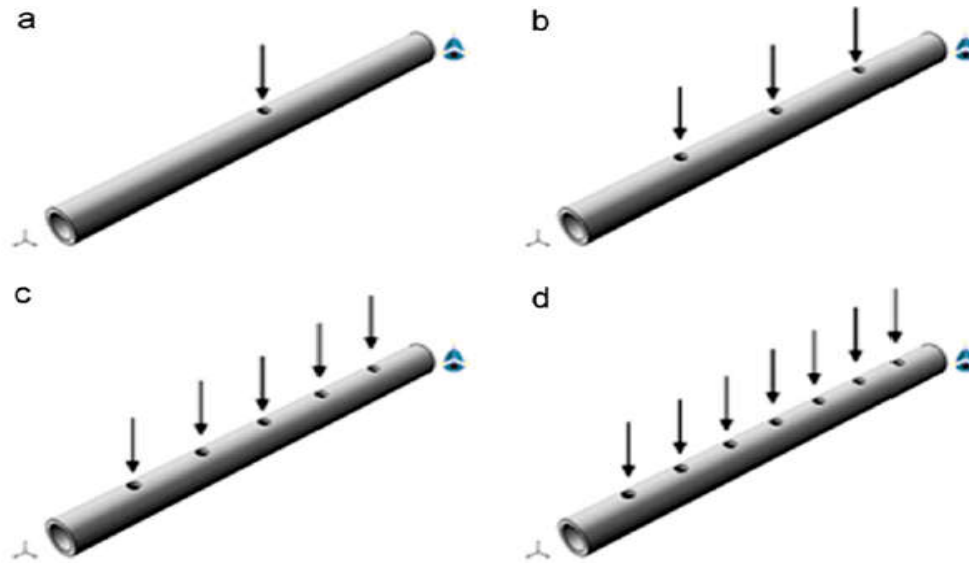


Fig.5 Layout of defects based on continuum structural approach (a) 1-defect, (b) 3-defect, (c) 5-defect, (d) 7-defect, [2].

STRUCTURE OF SINGLE WALLED CARBON NANOTUBES

The bonding in the CNTs is sp^2 , with each atom connected to three neighbors as in graphite. Carbon nanotubes are categorized as tube formed by rolling a sheet of Graphene about \vec{T} vector as shown in Fig. 6. The vector perpendicular to \vec{T} is the chiral vector denoted by \vec{C}_h . The chiral vector and the corresponding chiral angle define the type of CNT i.e. Armchair, zigzag, chiral. \vec{C}_h can be expressed with respect to two base vectors \vec{a}_1 and \vec{a}_2 as under

$$\vec{C}_h = n\vec{a}_1 + m\vec{a}_2 \tag{1}$$

Where n and m are the lattice translation indices, which decide the structure of the carbon nanotubes. Fig.6 represent the indices of translation (n,m) along with the base vectors, \vec{a}_1 and \vec{a}_2 . When the chiral angle $\theta = 0^\circ$ and the one of translation indices become equal to zero i.e. $m = 0$ then the form of the nanotubes is known as zigzag and when this angle have the value $\theta = 30^\circ$ and the translation indices are equal i.e. $n = m$ then the form of nanotube is known as armchair. For chiral form of carbon nanotube pair of indices (n, m) and the angle of chirality lies between 0° to 30° , where $n \neq m$.

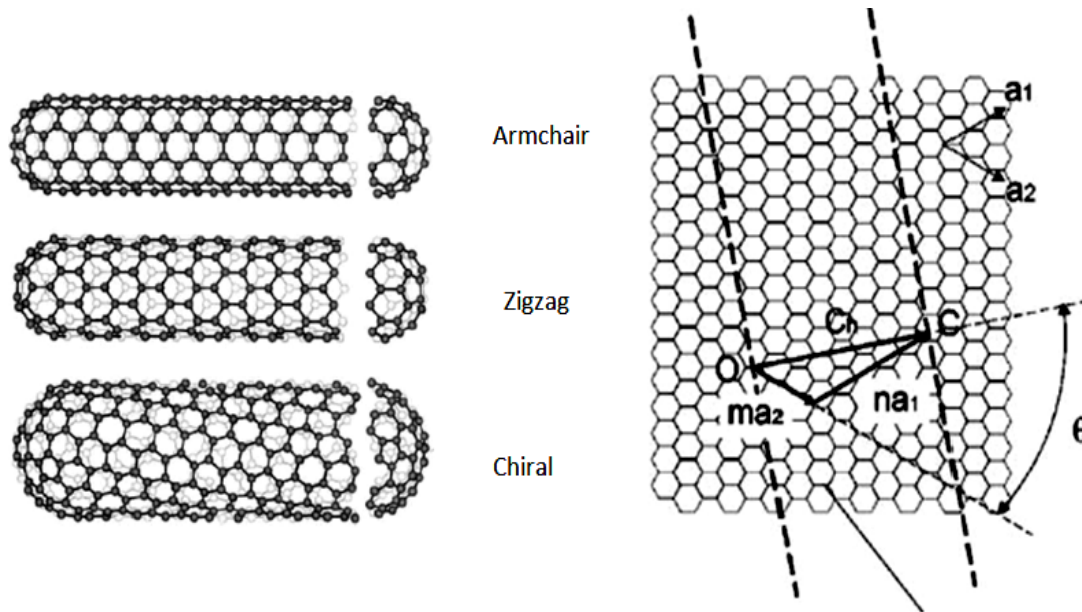
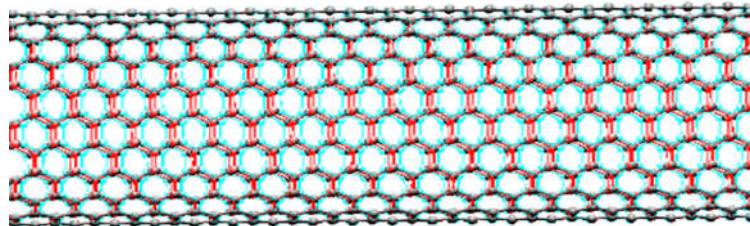


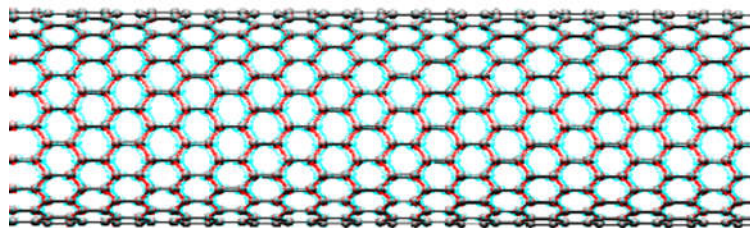
Fig.6 Hexagonal lattice of Graphene sheet including base vectors [28]

Atomic finite element modeling of single-walled carbon nanotube

A finite element model consisting of beam elements and concentrated mass is employed and the vibrational characteristics of cantilevered CNTs are explored. The elastic properties of the beam elements are calculated to consider the interatomic covalent bond between carbon atoms. The concentrated masses which represent the mass of the carbon atoms are placed at the end of the beams, which represent covalent bond between the carbon atoms. Fig. 7(a) and (b) represent (11, 11) and (19,0) carbon nanotubes with beam elements at point masses respectively.



(a) (11,11)



(b) (19,0)

Fig. 7. Atomic finite element model of (11,11) and (19, 0) SWCNTs with beam elements and point masses.

Armchair and zigzag CNTs have been utilized and their vibrational behavior with number of different vacancy defects and their different position along the length of CNTs has observed. The artificial defects are created uniformly along the length of CNTs. Two types of vacancy defects have been considered; 6-atoms vacancy defect and 24-atoms vacancy defects. 6 atoms and 28 atoms are removed to create 6atoms and 24 atoms vacancy defects respectably as shown in Fig.2.

The atomistic finite element model used for these CNTs is described here as under. Total strain energy of the system considering small deformations and omitting electrostatic interactions can be described as [29]

$$U_{total} = \sum U_S + \sum U_B + \sum U_T \tag{2}$$

Where U_S is bond stretching energy, U_B is the bond angle bending and U_T is the bond torsional energy which can be expressed as

$$U_S = \frac{1}{2}k_r(R - R_0)^2 = \frac{1}{2}k_r(\Delta R)^2 \tag{3}$$

$$U_B = \frac{1}{2}k_\theta(\theta - \theta_0)^2 = \frac{1}{2}k_\theta(\Delta\theta)^2 \tag{4}$$

$$U_T = \frac{1}{2}k_\phi(\Phi - \Phi_0)^2 = \frac{1}{2}k_\phi(\Delta\Phi)^2 \tag{5}$$

where k_r , k_θ and k_ϕ are the bond stretching, bond angle bending and torsional resistance force constants respectively, while ΔR , $\Delta\theta$ and $\Delta\Phi$ represent the bond stretching increment, bond angle variation bond twisting angle variation respectively as shown in Fig.8.

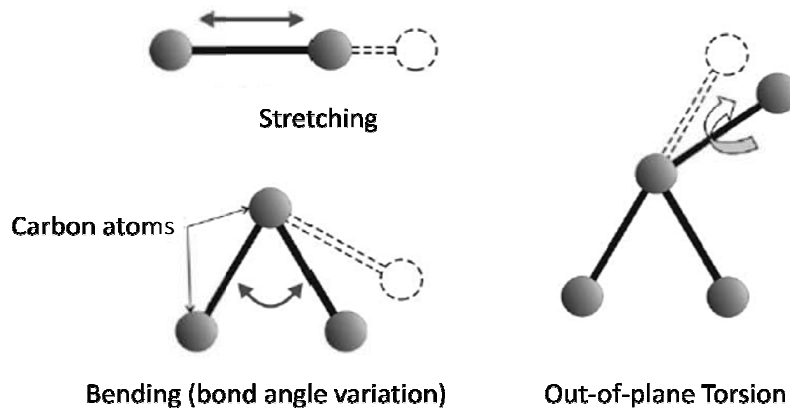


Fig. 8 Interatomic interactions in molecular mechanics [28]

The independency of the potential energies based on molecular mechanics can be observed. The elastic strain energy of a uniform beam subjected to an axial load can be given as

$$U_S = \frac{EA}{2L}(\Delta L)^2 \tag{6}$$

Where A is the cross sectional area, L is the length, ΔL is the change in the length and E is the Young's Modulus of the beam.

Strian U_B and U_T due to bending load and pure torsion load is given below

$$U_B = \frac{EI}{2L} (2\alpha)^2 \tag{7}$$

$$U_T = \frac{GJ}{2L} (\Delta\beta)^2 \tag{8}$$

where I is the moment of inertia, α is the relative bending angle of beam ends, is the relative rotational angle of the two ends. G is the Shear Modulus and J is the polar moment of inertia. As the potential energy is independent, energy equivalence of the stored energy of the molecular mechanics approach reveals [30]

$$\frac{EA}{L} = k_r \tag{10}$$

$$\frac{EI}{L} = k_\theta \tag{11}$$

$$\frac{GJ}{L} = k_\phi \tag{12}$$

The elastic properties of the beam element are given as [31]

$$d = 4 \sqrt{\frac{k_\theta}{k_r}} \tag{13}$$

$$E = \frac{k_r^2 L}{4\pi k_\theta} \tag{14}$$

$$G = \frac{k_r^2 k_\phi L}{8\pi k_\theta^2} \tag{15}$$

Where d is the diameter of the beam element.

To model the space frame structure of SWCNT, the elastic beam properties are applied to an elastic beam element and the mass properties to the point mass. The beam element length is taken equal to the distance of the covalent bond between two carbon atoms in the graphene sheet as CNT considered as a space frame structure. Neglecting the radii of the carbon nuclei, the radii of the carbon atoms are taken as 2.7×10^{-5} Å. Mass of the carbon nuclei which is positioned at the end of each beam element is considered as 1.99×10^{-26} kg. In present paper elastic properties of beam element are considered for analysis given in Table.1.

Table 1 Properties of beam element of space frame structure of SWCNT

Young's Modulus, E	5.49 TPa
Shear Modulus, G	0.871 TPa
Diameter, d	0.147 nm
Length of beam, L	0.142 nm
Poison Ratio, v	0.196

In this analysis, masses of the electron are assumed be insignificant in comparison with the nuclei.

Validation of atomistic finite element model

To validate the present finite element model based on molecular structural mechanics approach, the obtained results are compared with results of Joshi et. al. [2] and Hirai et. al. [21] for same geometric configuration boundary conditions of CNTs. Joshi et. al. [2] utilized continuum structural mechanics approach, where as Hirai et. al. [21] utilized molecular structural mechanics approach based on Tersoff-Brenner potential model to investigate the influence of number of defects on vibrational characteristics of SWCNTs. Effect of type of defects i.e. A type and B type, has also been examined. Geometric configuration has been used 1.5 nm diameter, 15 nm long [2] and 1.5 ± 0.01 nm diameter, 15 ± 0.01 nm long of armchair (10, 10) configuration [21] with cantilever boundary constraint. SWCNTs (11, 11) having same geometric configuration is utilized in present analysis with same end constraint. A comparison of results obtained in present study and the results of previously published research papers are shown in Fig. 9.

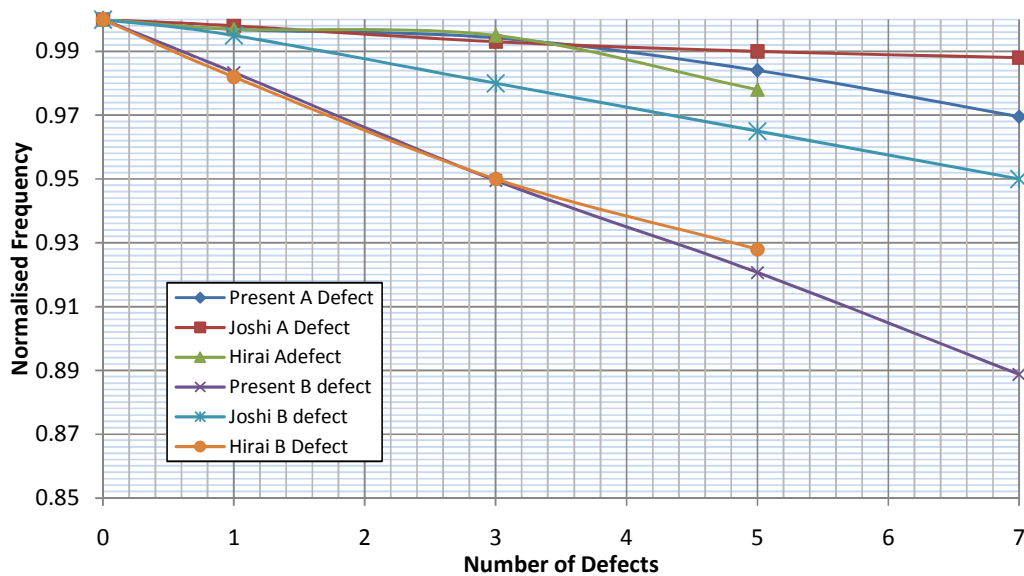


Fig.9. Comparison of variation in normalized frequency of SWCNT between the present paper, Hirai et al. [21] and Joshi et al. [2] with A and B types of number of atomic vacancy defects for $d = 1.5$ nm and $L = 15$ nm.

It is observed from the Fig.9 that present results have close proximity with Hirai et al. [21], but comparatively more variations has been observed with Joshi et. al.[2]. The similarity between present and Hirai et al. [21] is because of same approach and variations with Joshi et al. are due to fact that, the approach adopted by them was continuum structural mechanics. The results of continuum structural mechanics approach are based on the assumptions that there is no effect of the chirality (zigzag, armchair or chiral) on the effective wall thickness and the nanotube is assumed as a continuum solid tube. While the present molecular structural mechanics based finite element modeling approach easily incorporates the chirality (armchair (11, 11) for the present study) and the nanotube can be simulated such that the proximity of the real atomic structure can be retained. It is clear that molecular structural mechanics approach is more accurate with fewer assumptions than continuum structural mechanics approach.

Results and Discussion

The influence of number of different types of vacancy defect (type A and type B) for the cantilever configuration of SWCNT is analyzed by considering the normalized frequency of armchair (11, 11) and zigzag (19, 0) form of SWCNTs. The different positions (0.1, 0.3, 0.5, 0.7 and 0.9 of the length) of different types of vacancy defect are considered along the length of the SWCNTs from fixed end of nanotube. The analysis is carried out for different aspect ratios (10, 15 and 20) and the results for various aspect ratios and number of defects is represented in Fig.9. For armchair (11,11) CNTs with 'type A' defects, small variation in the normalized frequency of different armchair nanotubes is observed up to three defects, but this variation goes on increasing with number of defects, which is clearly shown in Fig 10(a). This is because of shifting of vacancy defects nearer to fixed end of nanotube due to increase in vacancy defects, which degrade the stiffness of the armchair SWCNTs. The maximum reduction is observed in smaller SWCNT. A similar trend is observed for type B defect with the difference of large frequency reduction with more than one defect as shown in Fig.10 (b). However normalized frequency of the zigzag (19, 0) with type A defect, increases with corresponding change in number of defects on nanotubes. Smaller is the length of zigzag nanotubes; higher is the change in normalized frequency with change in number of vacancy defects. This is due to the mass reduction dominating over the stiffness reduction with increase in number of vacancy defects, which is represented in Fig.10 (a). Whereas for type B defects zigzag nanotubes follow a similar trend as armchair having type B defects, with smaller frequency reduction represented in Fig.10 (b). Normalized frequency of (11,11) nanotubes decreases with increase in number of type A defect, whereas normalized frequency of (19,0) nanotubes increases with corresponding change in number of type A defect for different aspect ratios. Normalized frequency of (11,11) nanotubes decreases with increase in number of type B defect. The variation in normalized frequency of smaller nanotube is slightly higher than longer nanotubes, whereas (19,0) nanotubes have higher normalized frequency than (11,11) nanotubes for the defects considered in this paper.

An increase in natural frequencies observed, when position of the vacancy defect (type A and type B) shifting away from fixed end of cantilevered nanotube due to large variation in stiffness. At the position of the defect nearer to the fixed end of armchair (11,11) nanotube, the natural frequency due to type B defect is lower than type A defect for aspect ratio 10. And this difference in natural frequencies decreases as the position of defect shift away from the fixed end along the length of nanotube. It is also observed that, when the defect is within 0.45 to 0.6 of the nanotube length range, the natural frequencies of type A defective and type B defective armchair nanotubes have same natural frequency. As the defect position shift beyond this position towards free end, then natural frequency of nanotube due to type B defect is higher than type A defect. The reason for the lower natural frequency due to type B defect near the fixed end is comparatively higher loss of structural rigidity (Stiffness) of SWCNT than type A defect.

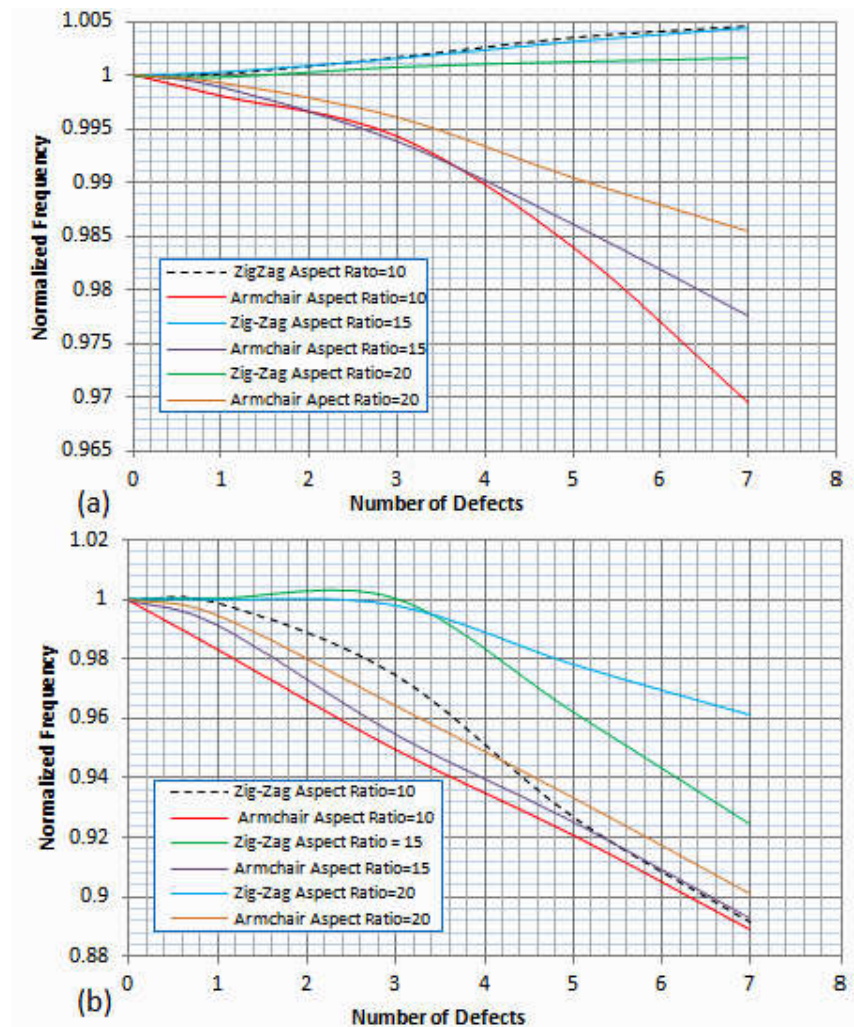


Fig. 10 Variation of normalized frequency of (11,11) and (19,0) SWCNTs with number of defects for (a) type A and (b) type B defects.

The natural frequency of both armchair and zigzag SWCNT are compared for different type of defects created at different position along the length of nanotube. It is observed that for armchair (11, 11) nanotube, the effect of type B defect is more prominent than type A defect if the position of defect is nearer to the fixed end and no significant change in natural frequency due to type of defects is observed when defect is nearer to mid position of nanotube. The same phenomenon is observed for zigzag (19, 0) nanotube but with lower natural frequency as compared to armchair nanotube with type A defect. The same variations is observed for different aspect ratios of 15 and 20 as shown in fig.12 and 13 respectively but for higher aspect ratio it is found that the difference in natural frequency for the both nanotubes for different types of defects reaches its minimum value at position of defects closer to free end.

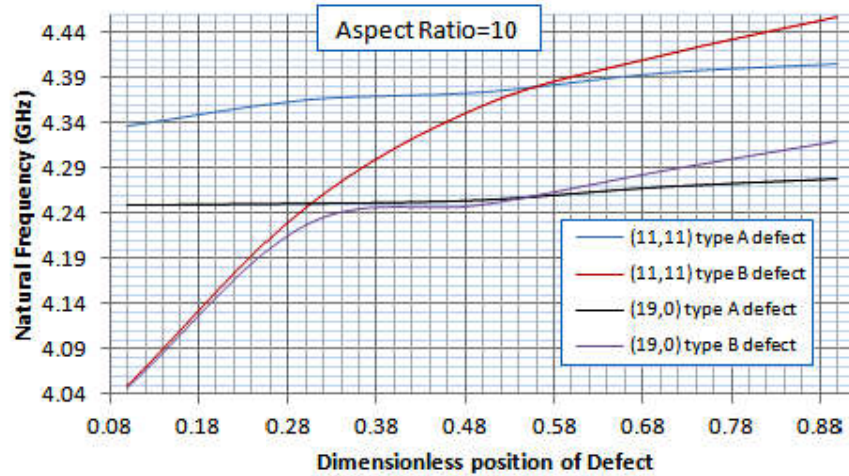


Fig. 11 Variation of natural frequency of armchair (11,11) and zigzag (19,0) nanotubes with position of type A and type B defects along the length of nanotubes of aspect ratio $L/d = 10$.

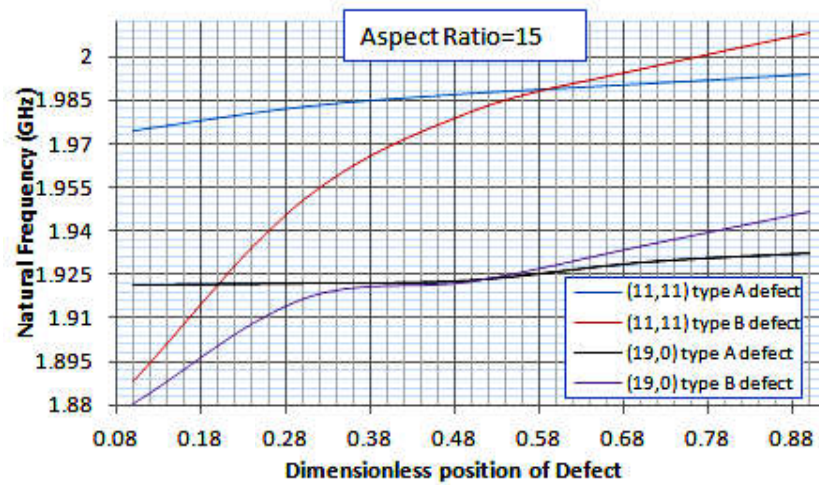


Fig. 12. Variation of natural frequency of armchair (11,11) and zigzag (19,0) nanotubes with position of type A and type B defects along the length of nanotubes of aspect ratio $L/d = 15$.

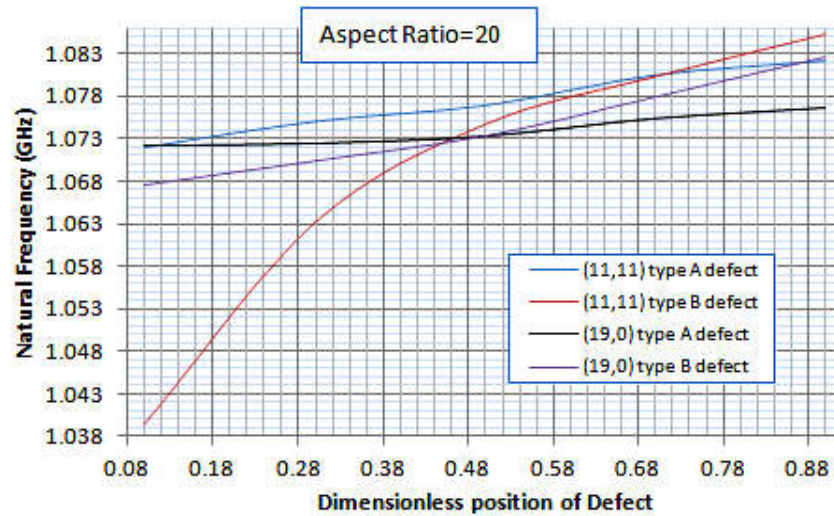


Fig. 13. Variation of natural frequency of armchair (11,11) and zigzag (19,0) nanotubes with position of type A and type B defects along the length of nanotubes of aspect ratio $L/d = 20$.

Fig. 14 represents the frequency shift due to the varying position of the defect along the length of the SWCNTs of armchair (11,11) and zigzag (19,0) form. It is observed that, the difference in the frequency shift due to type A and type B defects is higher, when the defect is nearer to fixed end. This difference gradually diminishes with varying position of defects from fixed end toward free end. At almost the middle of the length of the nanotubes difference in the frequency shift is zero. Then beyond this position this difference in frequency shift again increases. Frequency shift due to type A defect is lower than type B because of the large size of type B defect which leads to high reduction in structural stiffness of single-walled carbon nanotubes nearer to fixed end. The change in frequency shift is high for type B defect as it moves towards free end. Whereas this variation is very small for type A defect. At almost middle of the nanotube frequency shift are equal and frequency shift change its direction in negative zone beyond that point for armchair of aspect ratio 10. This means that, natural frequency of the defective nanotubes is higher than perfect nanotubes, because of dominance of structural mass loss over the structural stiffness reduction nearer to free end. Zero difference in frequency shift for armchair is shifted towards free end for higher aspect ratios as shown in Fig.14 (a), (d) and (f). A similar trend is followed in zigzag (19,0) form with zero frequency shift difference remains almost at the middle of the nanotubes for all aspect ratios. With change in aspect ratios of zigzag form of SWCNTs change in direction of frequency shift segregate to a single point instead of a range as shown in Fig. 14 (b), (c) and (e).

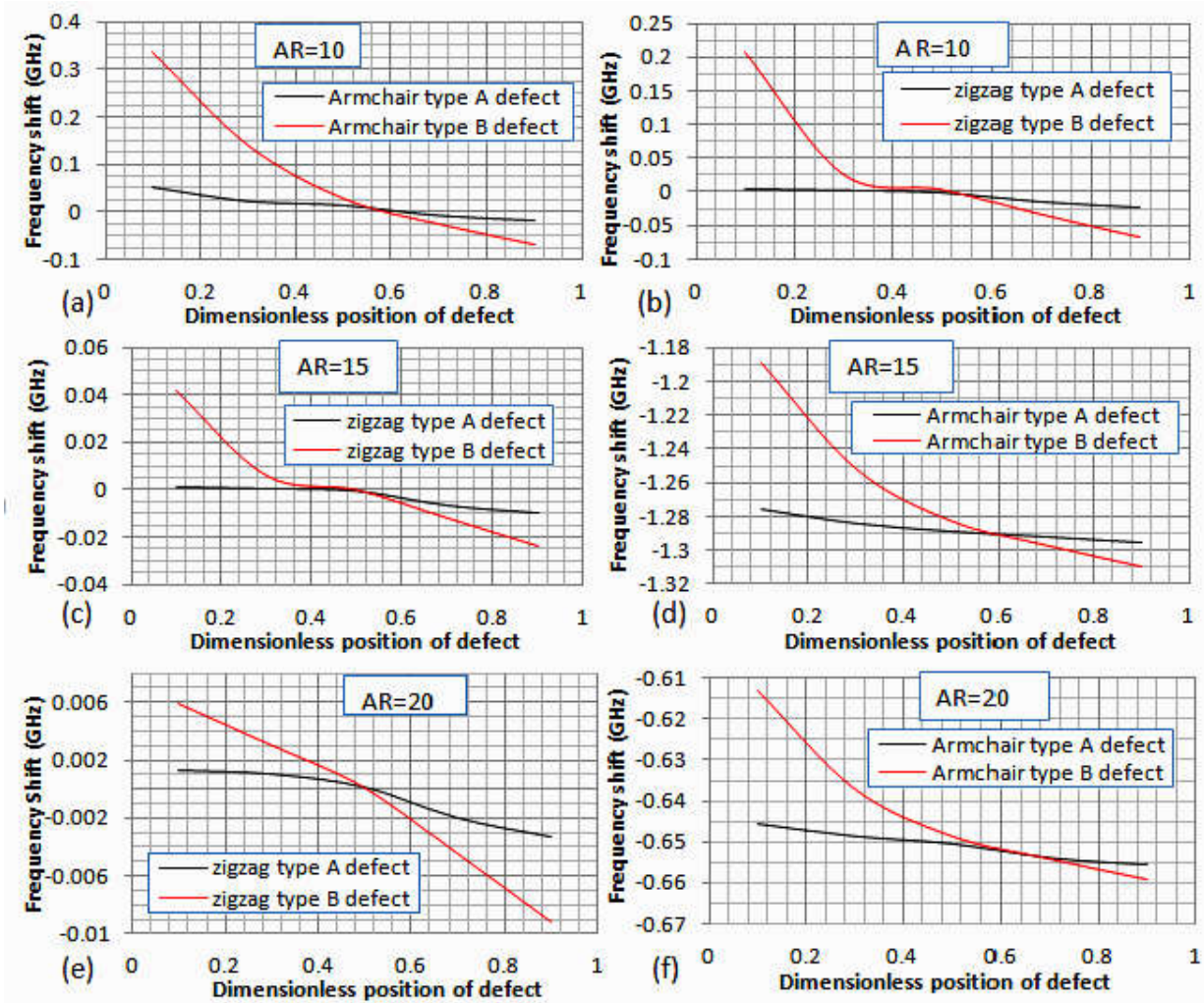


Fig. 14 Resonant frequency shift variation due to defect on the cantilevered configuration of armchair (11,11) and zigzag (19,0) form of SWCNTs, for different types of point defect (type A and type B) for their different dimensionless positions (0.1, 0.3, 0.5, 0.7 and 0.9 of the total length of the nanotube) for different values of considered aspect ratios.

CONCLUSION

Defective single-walled carbon nanotubes (SWCNTs) are modeled and analyzed using molecular structural mechanics approach in present work. An efficient atomistic finite element model is prepared with number of different atomic vacancy defect at various location of the SWCNTs of armchair and zigzag form and analyzed for dynamic behavior of these nanotubes. The influence of number, type and position of the defects along the length of SWCNTs of various aspect ratios, on vibrational characteristics has investigated in this paper.

The following concluding remarks are given on the basis of obtained results:

- Normalized frequency of armchair (11,11) nanotubes decreases with increase in number of type A defect, whereas normalized frequency of (19,0) nanotubes increases with corresponding change in number of type A defect for different aspect ratios. This is due to the mass reduction dominating over the stiffness reduction with increase in number of vacancy defects in zigzag (19, 0) tube. For 'type B' defects zigzag nanotubes follow a similar trend as armchair with smaller frequency reduction.
- Natural frequency of the armchair (11,11) form of nanotubes decrease with number of type A defects, whereas a rise is observed in zigzag (19,0) form of nanotubes. Type B defect has more influence than type A on natural frequency of both forms of nanotubes.
- Larger the size of the defect nearer the fixed end of cantilevered SWCNTs of both forms (armchair and zigzag), lower is the natural frequency. But same defect nearer to free end enhance the natural frequency of both armchair and zigzag form of SWCNTs.
- Smaller is the aspect ratio higher is the influence of atomic vacancy defects.
- It is also concluded that, the influence of the defects on natural frequency is whether adverse or favorable (in terms of natural frequency) depend on the position of the defect nearer to fixed or free end of the cantilevered SWCNTs.
- Finally it is observed that structural stiffness loss dominate over structural mass loss due to atomic vacancy defect nearer fixed end, whereas the situation becomes reverse if defect is nearer to free end of SWCNTs for armchair with both type A and type B defect and zigzag with type B defects only.

References

- [1] R.F. Gibson, E.O. Ayorinde, Y.F. Wen, *Composites Science and Technology* 67 (2007) 1–28.
- [2] A.Y. Joshi, S.C. Sharma, S.P. Harsha, *Physica E* 43 (2011) 1040–1045
- [3] C. Li, T.-W. Chou, *Phys. Rev. B* 68 (1–3) (2003) 73405.
- [4] R. Gao, Z.L. Wang, Z. Bai, W. de Heer, L. Dai, M. Gao, *Phys. Rev. Lett.* 85 (3) (2000) 622.
- [5] A. Y. Joshi, Satish C. Sharma, S.P. Harsha, *Int. J. Electrospun Nanofibers Appl.* 2 (3) (2008) 161.
- [6] A. Gupta, A.Y. Joshi, S.C. Sharma, S.P. Harsha, *IET Nanobiotechnology* 6 (2012) 115-121
- [7] R. Chowdhury, S. Adhikari, J. Mitchell, *Physica E* 42 (2009) 104.
- [8] S.L. Mielke, D. Troya, S. Zhang, J.-L. Li, S. Xiao, R. Car, R.S. Ruoff, G.C. Schatz, T. Belytschko, *Chem. Phys. Lett.* 390 (2004) 413.
- [9] S.K. Georgantzinos, N.K. Anifantis, *Computational Mechanics* 47 (2009) 168–177.
- [10] S.K. Georgantzinos, N.K. Anifantis, *Physica E* 42 (2010) 1795–1801.
- [11] M. Mir, A. Hosseini, G.H. Majzoubi, *Computational Materials Science* 43 (2008) 540–548.
- [12] A. Sakhaee-Pour, M.T. Ahmadian, A. Vafai, *Thin-Walled Structures* 47 (2009) 646–652.
- [13] T.W. Ebbesen, T. Takada, *Carbon* 33 (1995) 937.

- [14] S. L. Zhang, S. L. Mielke, R. Khare, D. Troya, R. S. Ruoff, G. C. Schatz, and T. Belytschko, *Phys. Rev. B* 71, (2005) 115403
- [15] S. Xiao and W. Hou, *Phys. Rev. B* 73, (2006)115406.
- [16] A. Stone and D. Wales, *Chem. Phys. Lett.* 128, (1986) 501.
- [17] A. Hashimoto, K. Suenaga, A. Gloter, K. Urita, and S. Iijima, *Nature London* 430, (2004) 870.
- [18] R. W. Haskins, R. S. Maier, R. M. Ebeling, C. P. Marsh, D. L. Majure, A. J. Bednar, C. R. Welch, B. C. Barker, and D. T. Wu, *J. Chem. Phys.* 127, (2007) 074708
- [19] V. Parvaneh, M. Shariati, H. Torabi, *Computational Materials Science* 50 (2011) 2051–2056
- [20] K.I. Tserpes, P. Papanikos, *Compos. Struct.* 79 (2007) 581.
- [21] Y. Hirai, S. Nishimaki, H. Mori, Y. Kimoto, S. Akita, Y. Nakayama, Y. Tanaka, *Jpn. J. Appl. Phys.* 42 (2003) 4120.
- [22] T. Belytschko, S. Xiao, G. Schatz, R. Ruoff, *Phys. Rev. B* 65 (2002) 235430.
- [23] S.K. Georgantzinou, G.I. Giannopoulos, N.K. Anifantis, *Comput. Mech.* 43 (2009) 731–741.
- [24] S. Kumar, S. P. Harsha, *Int. J. of Engg Research & Tech. (IJERT)* 2 (2013) 783-790.
- [25] D. Sanchez-Portal, E. Artacho, J.M. Soler, *Physical Review B* 59 (19) (1999) 12678–12688.
- [26] G Dereli, C. Ozdogan, *Physical Review B* 67 (3) (2003) 035416.
- [27] C. Li, T.-W. Chou, *Applied Physical Letters* 84 (1) (2004) 121–123.
- [28] K.I. Tserpes, P. Papanikos, *Composites: Part B* 36 (2005) 468–477
- [29] B.R. Gelin, Hanser/ Gardner Publishers, Cincinnati, OH, (1994).
- [30] K. Sohlberg, B.G. Sumpter, R.E. Tuzun, D.W. Noid, *Nanotechnology* 9 (1998) 30.
- [31] G.D. Mahan, *Physical Review B* 65 (2002) 235402.